university of groningen / faculty of science and engineering

A study on the influence of molecular hydrogen on Sn covered Cu using XPS

Bachelor thesis

Authors:
S. F. de Jong (S4129989)

Supervisor/Examiner:
prof. dr. ir. R. A. Hoekstra
Daily supervisors:
M. Salverda
dr. H. T. Jonkman
Second examiner:
dr. T. A. Schlathölter

July 8, 2023

Abstract

In this work, a study on the influence of molecular hydrogen gas on a Sn-covered Cu surface is discussed. The goal of the work is to set a benchmark for future research on the interaction between hydrogen gas and Sn deposited onto Ru. The study is relevant in the context of extreme ultraviolet (EUV) lithography, which requires the use of a hot Sn plasma to create EUV light for the fabrication of computer chips.

A Cu sample was prepared by cleaning it using various methods. Sn was then deposited onto the Cu sample, and X-ray Photoelectron Spectroscopy (XPS) was used to analyze the surface of the sample and determine the ratio of Sn to Cu for each deposition thickness.

The Sn-covered Cu substrate was then exposed to molecular hydrogen. The results showed that the hydrogen gas exposure did not have a significant effect on the percentage of elements present in the sample. From this, it could be concluded that the hydrogen gas was not effective in removing Sn from the Cu surface. The study also found traces of Zn contamination in the Sn filament used for deposition.

Further research is required to investigate the influence of molecular hydrogen on a Sn-covered Ru surface. It is expected that Ru will catalyze the formation of SnH_4.

Contents

1. Introduction

Following Moore's Law when making computer chips is crucial in today's quick-paced technological society, as it enables the fabrication of more powerful and efficient computing devices. According to Moore's law, the number of transistors in computer chips doubles every two years. Currently, computer chips are fabricated using extreme ultraviolet (EUV) lithography, for which light with a wavelength of 13.5 nm is required. With this wavelength, the needed integrated circuit of the computer chip can be etched into a silicon wafer [1]. The EUV light is created by an Sn plasma, resulting from irradiating Sn droplets with CO_2 laser pulses.

A consequence of creating EUV light from Sn plasma is that Sn debris can proceed to the light-collecting multilayer optics, which can compromise its reflectivity [2]. The reflectivity of the collector optics is crucial for chip fabrication. It is therefore important to limit the Sn debris that reaches the collector optics. Different methods have been proposed to prevent Sn debris damage. One of these methods is to use a hydrogen buffer gas. It is known that a hydrogen buffer gas can stop most of the Sn ions while maintaining a good transmission of EUV light. It is also clear that fast Sn ions are converted through recombination and/or charge transfer, while slow Sn ions are shown to form SnH_x molecules [3]. It is also known that a hydrogen buffer gas is more effective at stopping fast ions when the pressure is higher [4].

A buffer gas does not stop all Sn debris from reaching the collector optics. Atomic hydrogen can be used to etch the Sn from the collector optics surface while using the hydrogen buffer gas to create a local hydrogen plasma on the collector's surface. With this method, the collector optics can be cleaned without damaging it. In the process, the volatile gas SnH_4 is created which can be pumped out of the system [5].

It is currently not clear how a hydrogen gas interacts with Sn in the presence of Ru. Since Ru is known to dissociatively absorb hydrogen [6], it is suspected that the Ru surface will catalyze the formation of SnH_4. In this work, the interaction between hydrogen gas and Sn deposited onto a Cu surface will be examined using X-ray Photoelectron Spectroscopy (XPS). This will serve as a benchmark for future research into the interaction between hydrogen gas and Sn with Ru present.

2. Theory

2.1 Principle of XPS

X-ray Photoelectron Spectroscopy (XPS) can be used to perform surface analysis of a sample. Monoenergetic soft X-rays are incident onto the sample. The emitted electrons from the sample can then be detected. In this experiment, an Al Kα X-ray source will be used, for which the photons have an energy of 1486.6 eV. The photoelectric effect causes photoelectrons to be emitted. The emitted electrons can get detected with an energy close to their original kinetic energy until a depth of about 10 nm. Photoelectrons from a greater depth in the sample lose part of their energy through inelastic scattering processes and form a background in the XPS spectrum. The measured kinetic energy of the emitted electrons can be obtained by:

$$KE = h\nu - BE - \phi_s \tag{2.1}$$

where KE is the kinetic energy, $h\nu$ is the energy of the incident photon, BE is the binding energy of the atomic orbital from which the electron originates, and ϕ_s is the work function of the spectrometer.

With the measured kinetic energy, the known photon energy, and the work function of the spectrometer, the binding energy of the emitted electron can be found. Every element has a unique set of binding energies. XPS can thus be used to identify and quantify the elements present on and near the surface of the sample [7].

2.1.1 XPS spectra

The resulting spectrum from an XPS scan displays the count rate of the detected electrons versus their kinetic energy. With the known spectrometer work function and incident photon energy, the count rate can then be displayed versus the binding energy instead. Electrons can lose some of their kinetic energy before they are detected by inelastic scattering in the solid; this results in an increased background for binding energies higher than the actual binding energy of the electron [7].

There are different origins for the peaks that exist in the XPS spectra. The photoelectron lines are typically narrow and symmetric. The width of the photoelectron peak is dependent on the natural line width and the width of the X-ray line which creates the photoelectron. The instrumentation also has a contribution to the observed width of the peak [7].

Another type of peak that can be found in an XPS spectrum is that from the Auger lines. When a photoelectron is emitted, a hole is created, an electron with higher energy will occupy this vacancy, and its excess energy will be transferred to another electron which will then be emitted from the solid and can be detected. The Auger series is indicated by the initial and final vacancies in the transition. The kinetic energies of the Auger lines are independent of the incident photon energy. Because of this, they appear at different locations on the binding energy spectrum when switching to a different X-ray source [7].

When a nonmonochromatic X-ray source is used, some minor X-ray components with higher photon energies are also incident on the sample. Therefore, for every photoelectron peak, some peaks with lower binding energies can be found. These are so-called X-ray satellites [7].

When an atom has unpaired valence electrons, multiplet splitting can arise. After photoionization and after a hole is created in one of the core states, coupling can take place between the unpaired electron in the core state with an unpaired electron in the outer shell. This leads to a variety of final states, which can be detected in the XPS spectrum as multiple peaks, or as an asymmetric combined peak. This is not always as clearly visible because of the instrumental limitations [7].

When ions are created which are not in the ground state, they will have an energy above the ground state. This will give a reduced kinetic energy, and thus a higher binding energy. The difference between the binding energy of the peak resulting from the ground state and the peak resulting from the exited state will give the energy of the excited state. The resulting lines are called shake-up lines.

In Figure 2.1 a typical XPS spectrum of copper can be seen. The photoelectron lines are marked by their orbitals. The splitting of the 2p line is clearly visible at a binding energy of 933 eV and 953 eV, with a spin-orbit splitting of 20 eV. The peak next to the right of these two peaks is the satellite peak, which is there because a nonmonochromatic X-ray source is used.

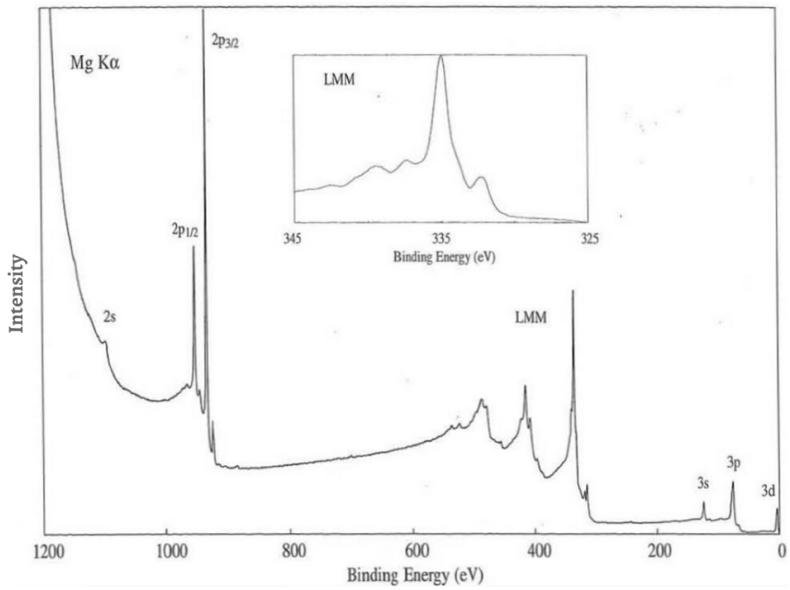

Figure 2.1: XPS spectrum of copper using an Mg Kα X-ray source [7].

2.1.2 Chemical shift

The chemical environment of a given element determines the exact binding energy. Any modification of an element's chemical environment will cause the valence electron charges to be spatially redistributed and thus alter the potential as experienced by the core electron. The potential of the core electrons is altered by this redistribution, which also alters the binding energies of the core electrons. This change in binding energy can be registered with the use of XPS [8].

2.1.3 Atomic sensitivity factor

In order to perform a quantitative analysis of XPS spectra, the atomic sensitivity factor is needed. Assuming a solid is homogeneous to a depth of several electron mean free paths, the count rate of detected electrons from an orbital of constituent atoms is given by:

$$I = nf\sigma\phi yAT\lambda, \tag{2.2}$$

where n is the number of atoms per cm^3 of the element, f is the flux of X-ray photons incident on the sample in photons cm^{-2} s^{-1}, σ is the photoelectric cross-section for a particular transition in cm^2 per atom, ϕ is the angular efficiency factor for the instrument arrangement, y is the rate at which photoelectrons of normal energy are produced in the photoelectric process, A is the area of the sample from which photoelectrons can be detected, T is the detection efficiency of the photoelectrons emerging from the sample, and λ is the mean free path of the photoelectrons in the sample.

For any photoelectron transition in an atom we can define the atomic sensitivity factor,

$$S = \sigma\phi yAT\lambda. \tag{2.3}$$

Then for any homogeneous solid the ratio of the number of atoms per element can be found using the count rate and atomic sensitivity factor (ASF):

$$\frac{n_1}{n_2} = \frac{I_1/S_1}{I_2/S_2}. \tag{2.4}$$

When comparing the atomic sensitivity factor for a certain atomic orbital for different instrument arrangements, the only parameter that is different for different arrangements in equation (2.3) is the angular efficiency factor ϕ. This factor is defined as follows:

$$\phi = \frac{dI}{d\Omega} = \frac{I_t}{4\pi}[1 - \frac{1}{4}\beta(3\cos^2\theta - 1)]. \tag{2.5}$$

Where $I_t/4\pi$ is the intensity expected per steradian if the emission is isotropic, θ is the angle between the photon and detected electron, and β is a characteristic parameter for each of the photoelectron interactions [9].

The measurements in this experiment are performed under an angle of 30° between the X-ray source and the electron analyzer. The available ASFs in literature are determined for an angle of 54.7° and 90°. In Table 2.1 the angular efficiency factor ϕ is given for each angle.

Table 2.1: Angular efficiency factor ϕ for relevant angles.

Angle	ϕ
90°	$I_t/4(1 + \frac{1}{4}\beta)$
54.7°	$I_t/4$
30°	$I_t/4(1 - 0.3125\beta)$

Since β is independent of the angle, it is constant for one atomic orbital. The ASF for 30° can thus be found by determining β from the two angles available in literature together with the ASF for 54.7°.

2.2 Principles of tapping mode AFM

Atomic force microscopy uses an extremely sharp tip on a probe. There are different modes that can be used, one of which is the tapping mode. The tip scans across the surface of the sample line by line, tapping the surface with the tip. The tip is attached to a cantilever beam which bends as the tip scans the surface. The amount of bending from the cantilever beam is registered with a laser diode and a detector. Oscillations close to the cantilever's resonance frequency are produced. The tip then exhibits what is referred to be a sinusoidal motion. When the sample is scanned, its Van der Waals forces will act upon the tip and alter the amplitude of the cantilever. The amplitude of the cantilever is kept constant using a feedback loop by changing the total height of the cantilever. With this height the heights on the sample can be determined, enabling line-by-line tracing of the sample's topography [10].

3. Experimental methods

3.1 Experimental setup

The complete experimental setup consists of a preparation chamber where the sample can be annealed, sputtered and different materials can be deposited onto the sample. There is also a hydrogen gas supply in the preparation chamber. The preparation chamber is separated from the measurement chamber, where the X-ray source and electron analyzer enable XPS measurements. The sample that will be used in the experiment is mounted onto a Mo sample holder, which can be entered into the preparation chamber with a separate loading dock. In Figure 3.1 an image of the setup can be seen.

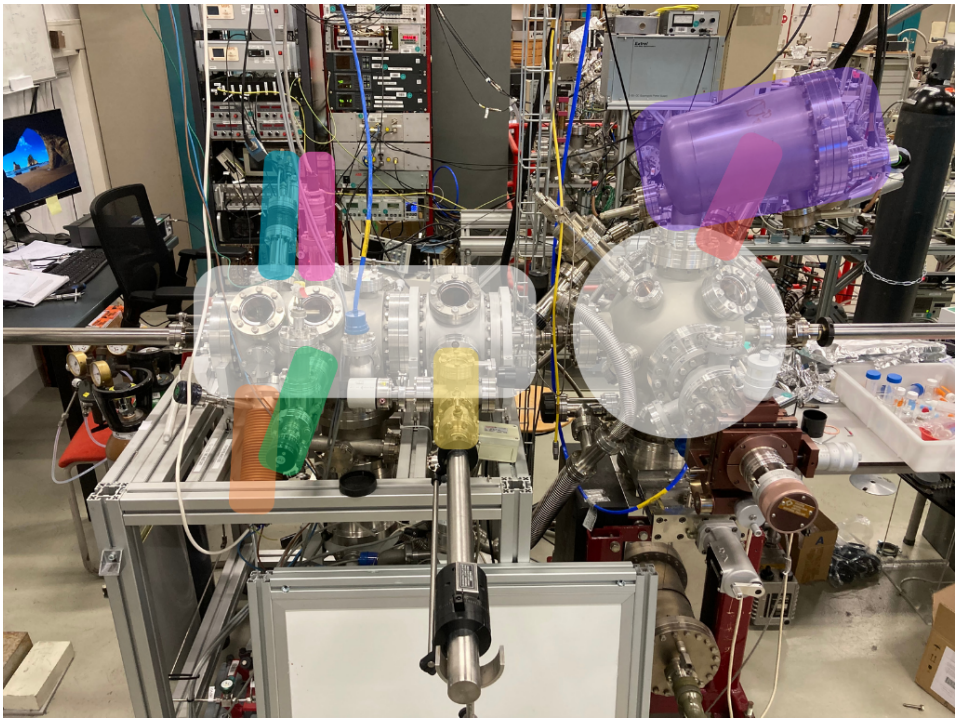

Figure 3.1: Image of the experimental setup for sample preparation and XPS measurements with the following components indicated by their color: The preparation chamber in white on the left side, the measurement chamber in white on the right side, the Knudsen Cell in orange, the quartz crystal microbalance in blue, the Ar-sputtering gun in pink, the annealing stage in green, the loading dock in yellow, the electron energy analyzer in purple and the X-ray source in red. The hydrogen gas supply is located at the back of the preparation chamber underneath the quartz crystal microbalance.

3.1.1 Measurement chamber

The measurement chamber of the XPS setup is kept at vacuum using an ion pump and a Ti sublimation pump. The chamber is equipped with a sample holder connected to a manipulator so that it can be moved to the optimal position to take measurements. The

sample holder is electrically connected to a DC power supply with a voltage output of 4 volts. This connection is made to compensate for the work function of the spectrometer and ensure accurate measurements.

The Al Kα X-ray source is operated at 10 kV and at an anode emission current of 5, 10, 20, or 34 mA. The X-ray source is mounted at an angle of 30° with respect to the electron-focusing lens of the electron energy analyzer. In Figure 3.2 a picture of the measurement chamber can be seen.

Figure 3.2: Image of the heart of the measurement chamber. From left to right a helium lamp, the entrance to the electron energy analyzer, and the X-ray source can be seen.

Straight above the sample holder the electron lens is located. This lens focuses the electrons from the sample to the entrance slit of the energy analyzer. The energy analyzer is a hemispherical analyzer. This analyzer has two hemispheres between which an electric potential can be maintained. The photoelectrons enter the hemispheres and are deflected by the electric field as they proceed toward the channeltron which is used to detect the electrons. A photoelectron with too much kinetic energy will not reach the detecting system as it will hit the top hemisphere. A photoelectron that does not have enough kinetic energy will hit the bottom hemisphere, and will thus also not reach the detecting system. The photoelectrons that reach the detecting system thus have a kinetic energy in a certain range, the pass energy. By varying the potential of the retarding plate the XPS spectrum can be taken over a range of binding energies. In Figure 3.3 a diagram of the XPS setup can be seen.

3.1.2 Preparation chamber

The preparation chamber is kept at vacuum with a turbo-pump and it is equipped with an annealing stage. In Figure 3.4 a copper sample can be seen on the annealing stage being heated to a temperature of 500 °C.

Above the annealing stage, the Ar sputtering gun is located which can be used for cleaning the sample. To execute the sputtering procedure, the preparation chamber is filled with Ar gas to a pressure of $1 \cdot 10^{-5}$ mbar. A voltage is supplied to the Ar gun which causes

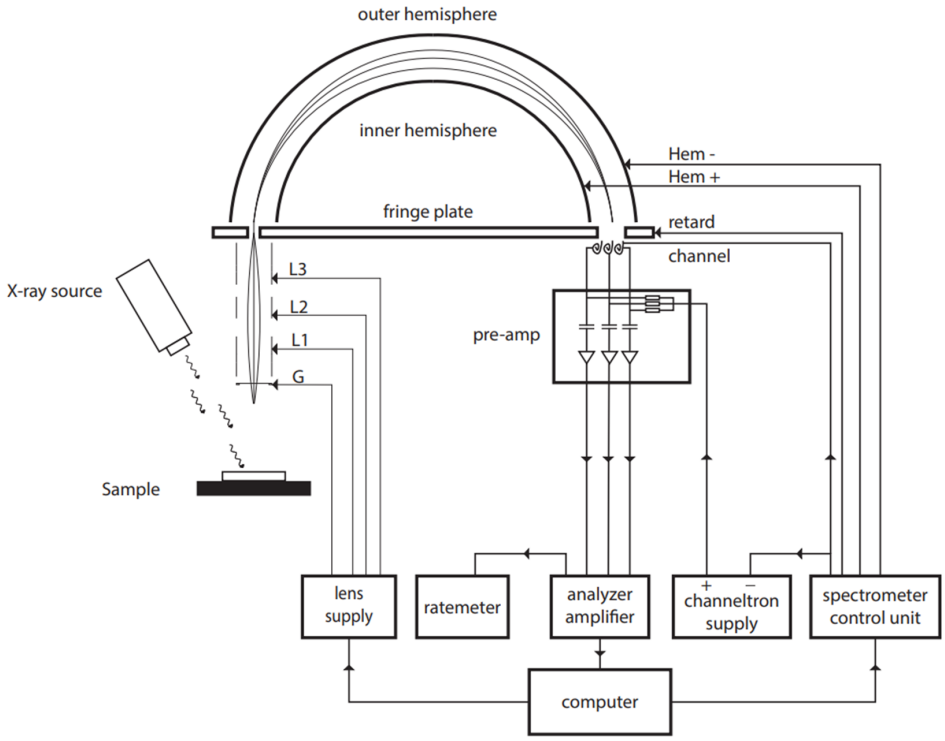

Figure 3.3: Diagram of hemispherical energy analyzer for an XPS application.

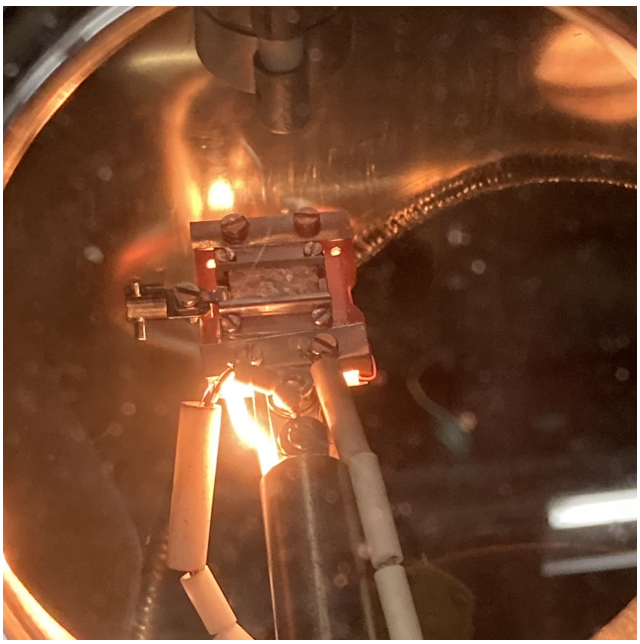

Figure 3.4: A copper sample in the sample holder, on the hot resistive theater filament of the annealing stage, heated to 500 °C. Above the annealing stage the Ar-sputtering gun can be seen.

the Ar ions to be accelerated toward the target where they collide with the surface atoms and molecules. A transfer of energy takes place that causes the struck atoms or molecules

to be ejected. These sputtered atoms or molecules can then freely move in the vacuum chamber and will be pumped out eventually. Since the sputtering gun is mounted above the annealing stage, sputtering and annealing can be performed simultaneously.

Sn can be deposited onto a sample in the preparation chamber, using a Knudsen cell. The cell contains a crucible made of Al_2O_3. The crucible contains Sn and should be heated to about 1030 °C to evaporate Sn.

Across the Knudsen cell in the preparation chamber, a quartz crystal microbalance (QCM) is located. It is used to measure the thickness of the deposited layer of Sn. The crystal has a certain resonance frequency which is constantly monitored. When Sn is deposited onto the crystal this resonance frequency decreases. With the known density and z-factor of Sn, the thickness of the deposited Sn layer can be determined from the changed resonance frequency. Before a deposition onto a sample, the flux of deposited Sn is determined with the QCM. With this flux, the duration of the deposition necessary for the needed thickness can be estimated.

A hydrogen gas supply is connected to the preparation chamber, with which the effect of hydrogen gas on the sample can be determined.

3.2 Methods

In this experiment, the effect of hydrogen on Sn deposited onto a Cu sample will be investigated. In order to do this, first a proper Cu sample is needed.

To make the Cu sample that is available for this experiment of sufficient quality, it has to be analyzed with AFM to determine its quality. Then it will be sputtered, annealed, cleaned with an O-plasma, exposed to air while being heated and a metal polishing will be used.

Once the Cu sample is of sufficient quality, a pre-determined amount of Sn can be deposited onto it while taking XPS spectra in between the depositions. The spectra are then fitted to determine the areas of the different peaks. With these areas, the ratio between the elements present in the sample can be determined. From these spectra the thickness of the deposited Sn is known, these spectra will thus serve as a reference for later measurements.

With the Sn deposited onto the Cu sample, it is attempted to remove the Sn with the H_2 gas. The XPS spectra before and after the H_2 exposure are compared, and the influence of the H_2 gas on the Cu-Sn sample is determined.

4. Results

4.1 Preparation of Cu sample

The surface of the Cu sample was initially examined using AFM. The resulting topography images can be seen in Figure 4.1. The depth profiles were measured through the highest and lowest areas diagonally across each topography image.

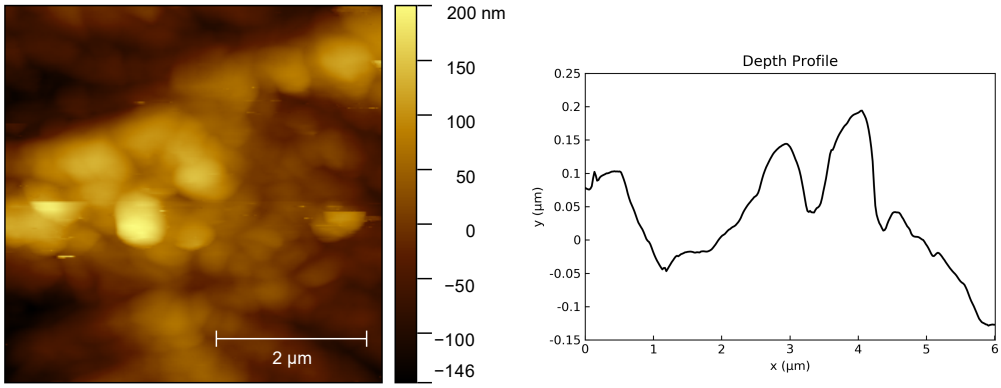

(a) AFM topography image

(b) Depth profile determined from (a)

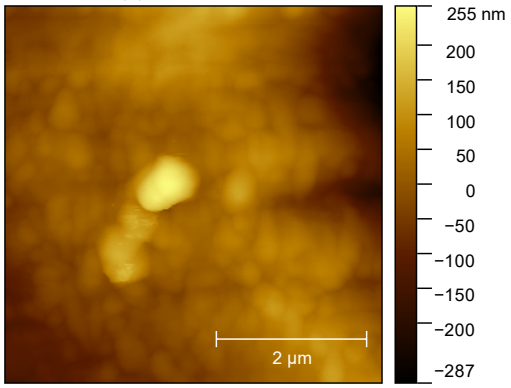

(c) AFM topography image

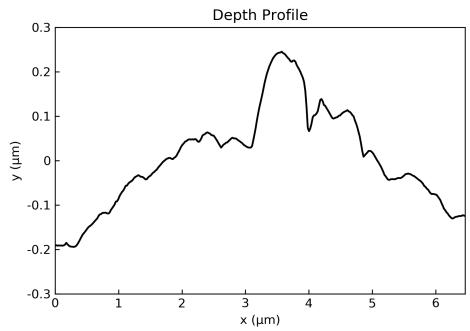

(d) Depth profile determined from (c)

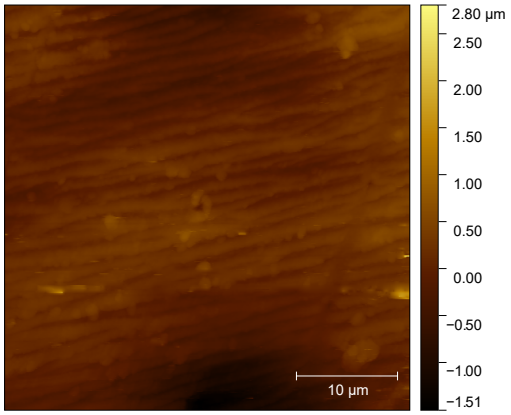

(e) AFM topography image

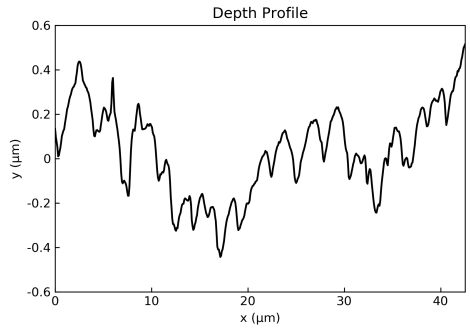

(f) Depth profile determined from (e)

Figure 4.1: AFM topography images and their depth profiles at different locations of the untreated Cu sample taken with AFM.

It was found that the surface variation was a few hundreds of nanometers in between the grain boundaries that can be seen from optical images of the sample. The height variation at these boundaries was too great to determine with AFM. In Figure 4.2 one of these images can be seen.

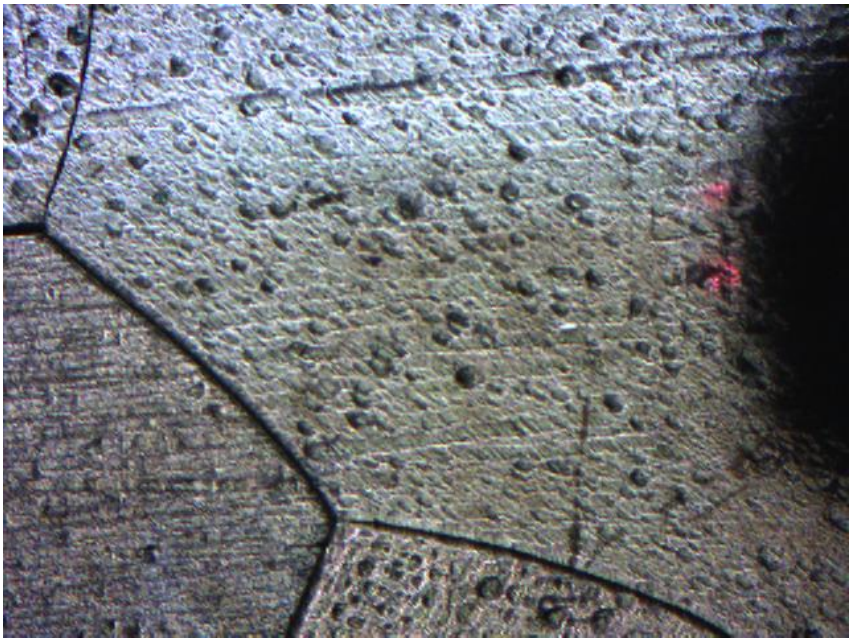

Figure 4.2: Optical image of Cu sample showing grain boundaries and rough surface structure. The cross-section of each grain is a few millimeters.

After the surface of the Cu sample was analyzed using AFM, it was Ar-sputtered for 3 hours. The XPS spectrum taken after sputtering can be seen in Figure 4.3a. After sputtering the sample was annealed for 2 hours at 600 °C. The XPS spectrum taken after annealing can be seen in Figure 4.3b.

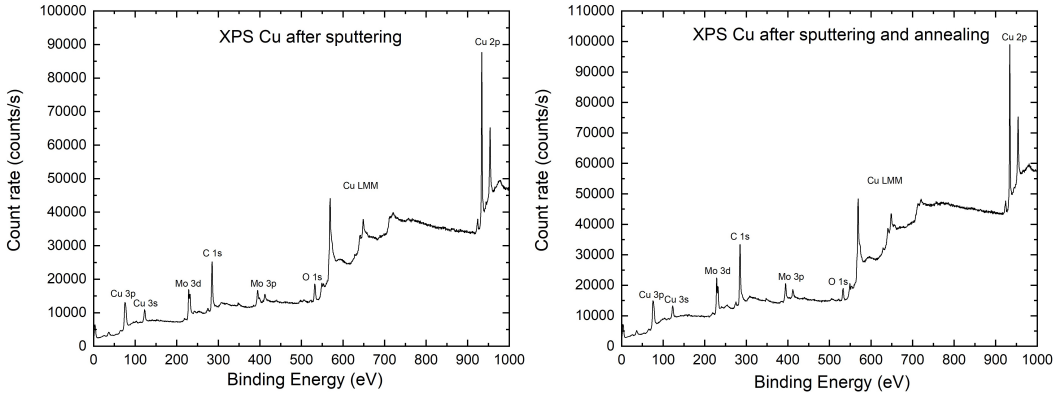

(a) (b)

Figure 4.3: XPS spectra of the Cu sample after subsequent (a) 3 hours of Ar-sputtering and (b) 2 hours of annealing at 600 °C.

From the spectra in Figure 4.3 it was determined that the quality of the substrate was insufficient as the contributions of the C 1s and O 1s peaks are relatively large compared to the Cu peaks. Considering the atomic sensitivity factors the amount of C is comparable to

the amount of Cu. The Mo contribution to the spectrum is due to the Mo sample holder. Because of the large C and O contributions the sample was cleaned using an O-plasma treatment, it was heated while exposed to air, and a metal polishing was used to remove C. The XPS spectra taken after applying these methods can be seen in Figure 4.4.

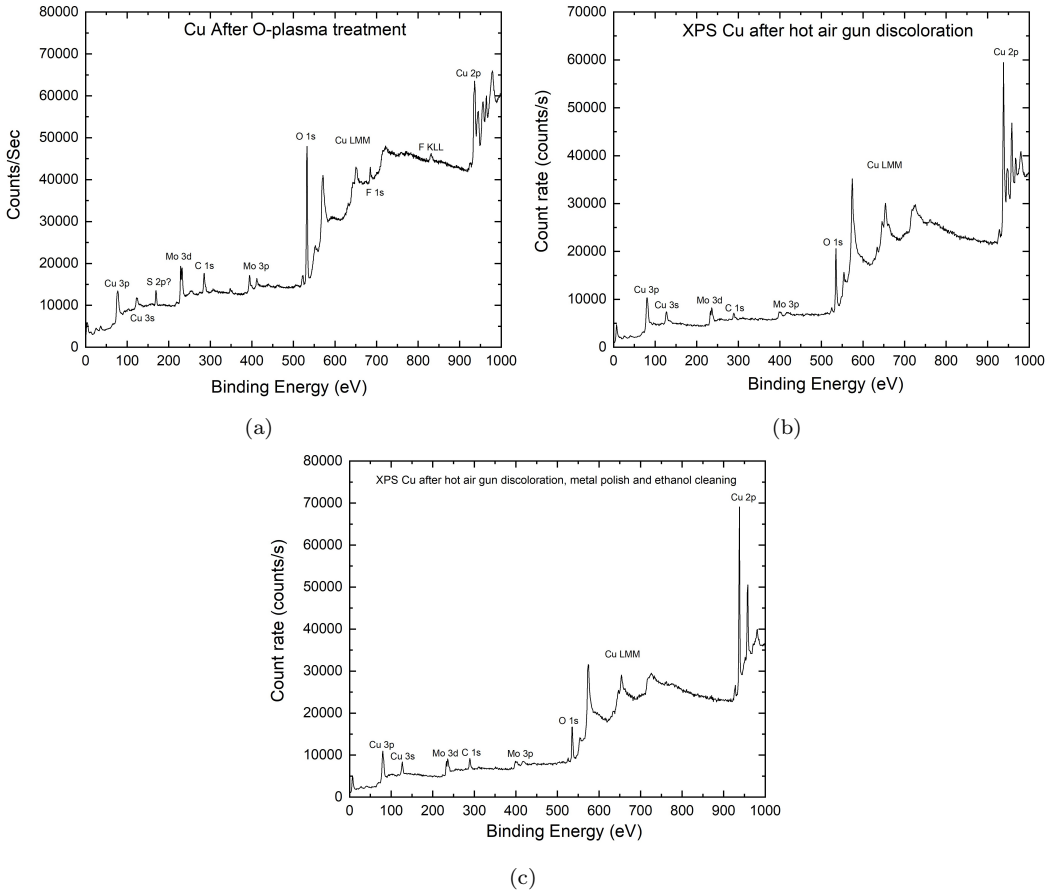

Figure 4.4: XPS spectra of Cu sample after subsequent (a) exposure to O-plasma, (b) hot air gun discoloration and (c) metal polishing.

From the spectra in Figure 4.4 it was determined that the C was removed sufficiently. However, more sputtering is necessary to remove the O. Therefore, the sample was first sputtered for 1.5 hours after which it was sputtered and annealed simultaneously for 1.5 hours at 700 °C. For the last 15 minutes of the simultaneous sputtering and annealing, the sputtering was terminated. In Figure 4.5 the subsequent XPS spectra after sputtering, and sputtering and annealing can be found.

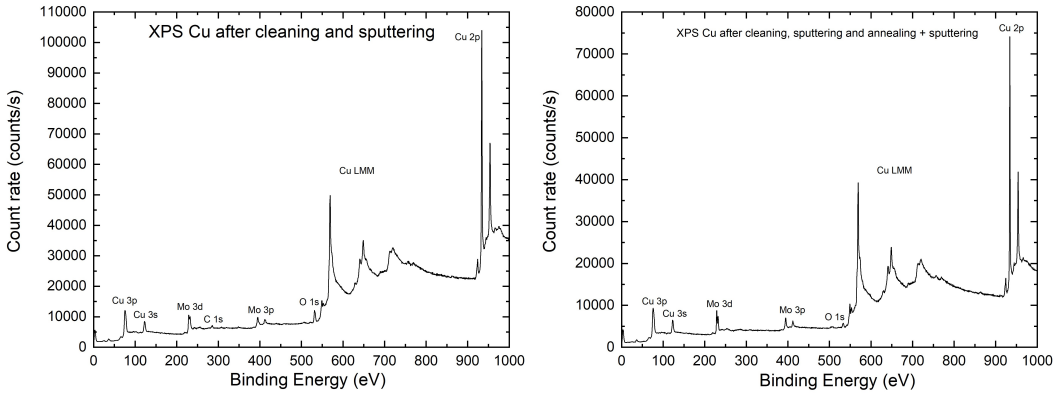

(a) (b)

Figure 4.5: XPS spectra of Cu sample after subsequent (a) 1.5 hours of Ar-sputtering and (b) 1.5 hours of simultaneous Ar-sputtering and annealing at 700 °C.

To conclude, the procedure used to create pure Cu substrates is as follows:

- The substrate was Ar-sputtered for 3 hours.
- The substrate was annealed at 600 °C for 2 hours.
- The substrate was cleaned using an O-plasma treatment.
- The substrate was heated while being exposed to air.
- The substrate was cleaned using a metal polishing solution.
- The substrate was cleaned with ethanol.
- The substrate was Ar-sputtered for 1.5 hours.
- The substrate was Ar-sputtered and annealed at 700 °C simultaneously for 1.5 hours. For the last 15 minutes the sputtering was terminated.

After these cleaning methods were all applied it was concluded that the intensity of the C 1s and O 1s peaks had decreased sufficiently for this experiment. To check the surface roughness, the sample was again examined at different locations on the sample using AFM. The results can be found in Figure 4.6. Two additional AFM measurements can be found in Appendix A.2.

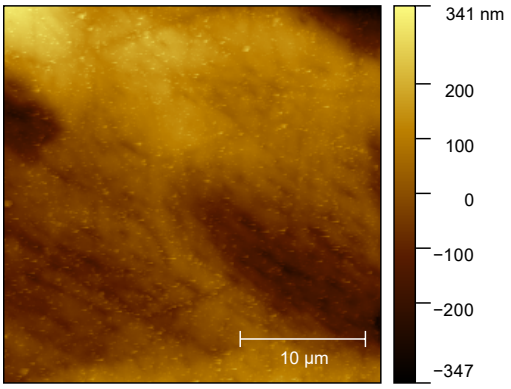

(a) AFM topography image

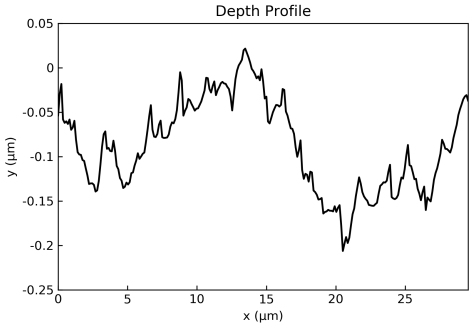

(b) Depth profile determined from (a)

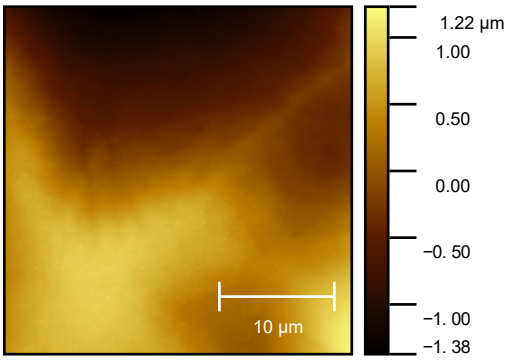

(c) AFM topography image

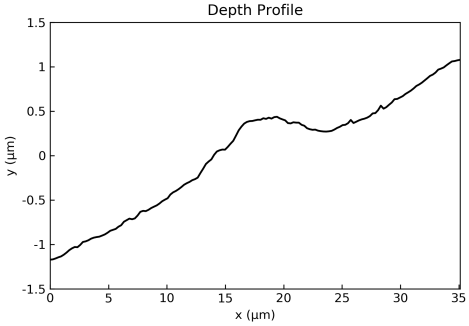

(d) Depth profile determined from (c)

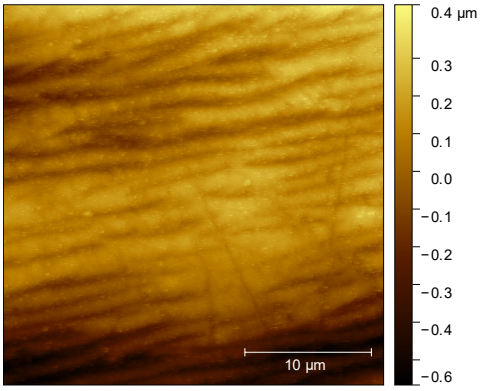

(e) AFM topography image

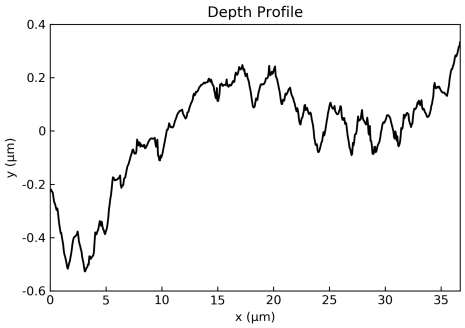

(f) Depth profile determined from (e)

Figure 4.6: AFM topography images and their depth profiles at different locations of the cleaned Cu sample taken with AFM.

From the AFM measurements, it was determined that the variation in height was still significant after sputtering annealing and other cleaning methods. It was decided to start Sn deposition after taking another XPS spectrum. This spectrum can be found in Figure 4.7. It can be seen that the C and O contributions increased after the AFM examination, this is most likely due to the exposure to air. Since the presence of C and O are not expected to influence the experiment significantly, no further cleaning methods will be applied to the sample.

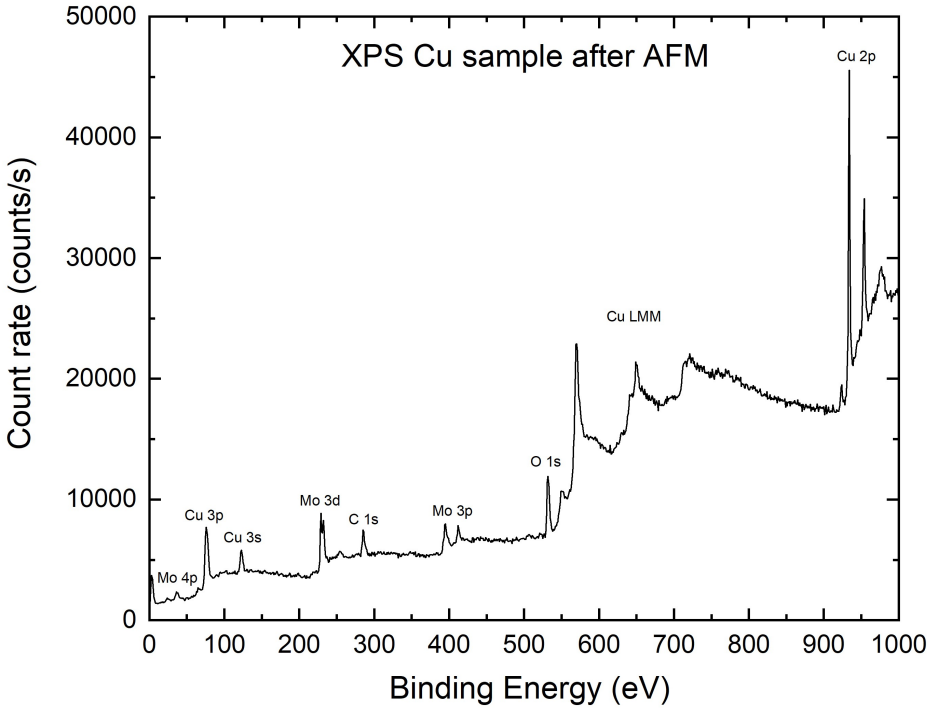

Figure 4.7: XPS spectrum of the cleaned Cu sample after AFM examination.

4.2 Sn deposition onto Cu sample

XPS spectra were taken before and after four Sn depositions which have an estimated thickness of 12Åeach. This was done in order to calibrate which thickness of Sn on the Cu sample corresponds to what ratio of Sn/Cu is found from the XPS spectra. The resulting XPS spectra can be found in Figure 4.8. It can be seen that there are peaks present that correspond to Zn, which led to the discovery that the Sn which is evaporated in the Knudsen cell was contaminated with Zn. In Appendix A.3 the XPS spectrum of a Sn pellet similar to the filament of the Knudsen cell can be seen where minor traces of Zn were found.

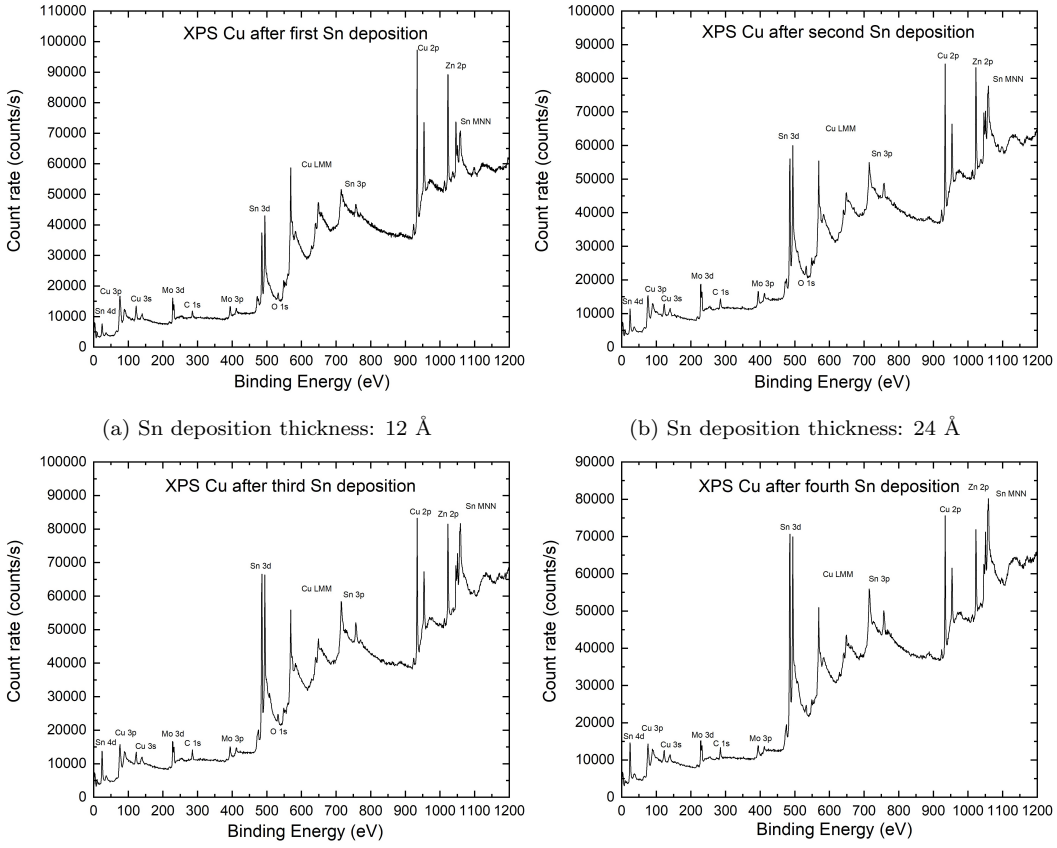

(a) Sn deposition thickness: 12 Å

(b) Sn deposition thickness: 24 Å

(c) Sn deposition thickness: 36 Å

(d) Sn deposition thickness: 48 Å

Figure 4.8: XPS spectra of Cu sample taken after consecutive Sn depositions of 12 Å.

The XPS spectra from Figure 4.8 can be fitted using the XPSPEAK41 software. With this software, a Shirley background can be applied to account for the detected background. In Figure 4.9 such a fit can be seen for the Cu and Zn peaks from the XPS spectrum taken after the first Sn deposition. From the fit, the area, FWHM, and percentage of Gaussian and Lorentzian of the curve can be found, as seen at the top left of Figure 4.9. The Lorentzian shape of a peak can be attributed to the line width of the X-ray source. A more Gaussian shape of a peak can be due to different broadening mechanisms like vibrations in the material [11].

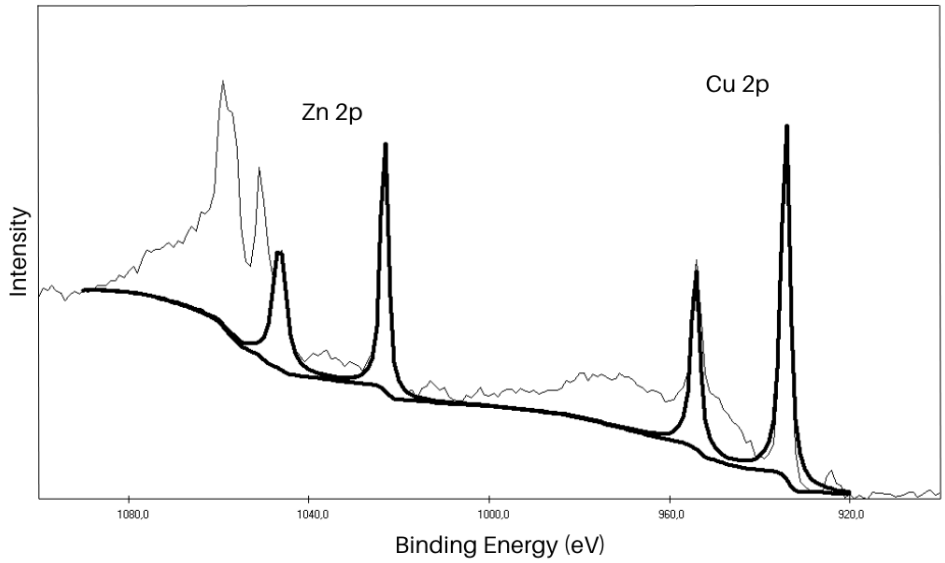

Figure 4.9: XPSPEAK41 fit with a Shirley background of the Cu 2p peaks at 933 eV and 953 eV and the Zn 2p peaks at 1022 eV and 1045 eV.

This fitting technique is applied to all relevant peaks. Their images can be found in Appendix A.4. The areas of the peaks correspond to the total count rate associated with that peak. Using equation (2.3) and the atomic sensitivity factors provided in Appendix 2.1.3, a relative number of atoms of one element with respect to the number of atoms of another element can be determined. In Figure 4.10 the percentage of each element detected with XPS is displayed for each Sn deposition thickness.

The most important ratio between elements in the sample is the ratio of Sn/Cu. A plot of this ratio with respect to the estimated Sn deposition thickness can be found in Figure 4.11.

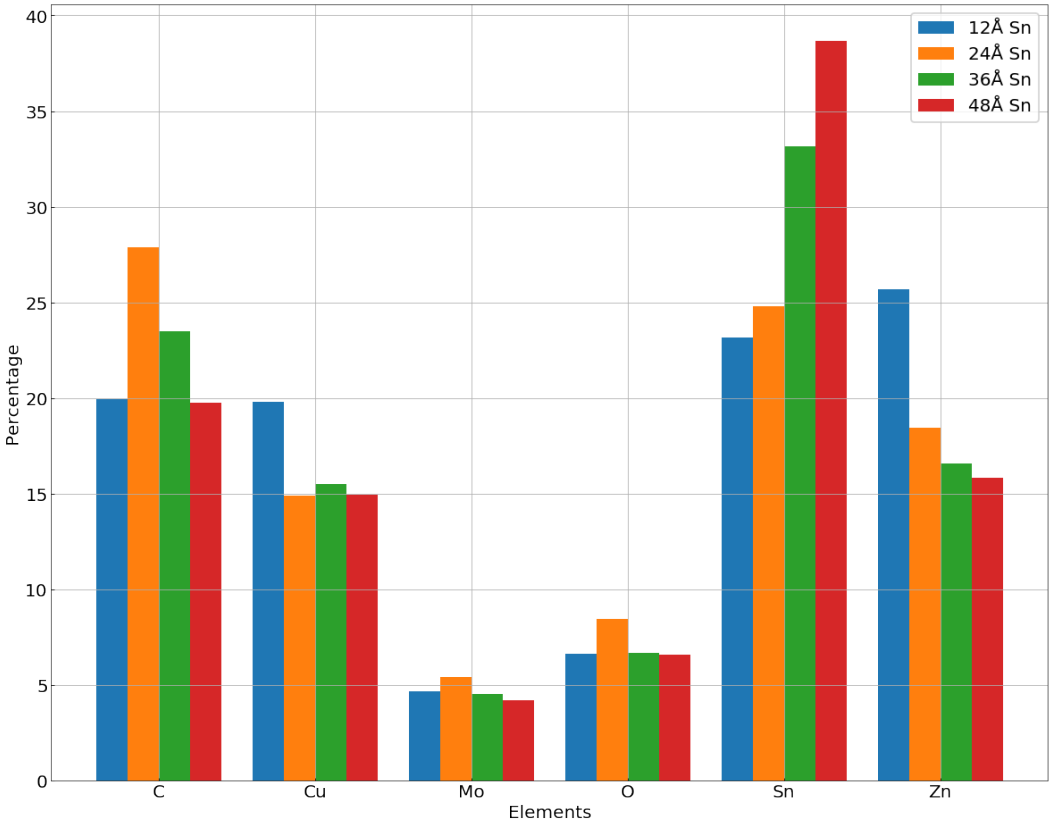

Figure 4.10: Histogram with percentages of elements measured for the consecutive Sn depositions of 12 Å.

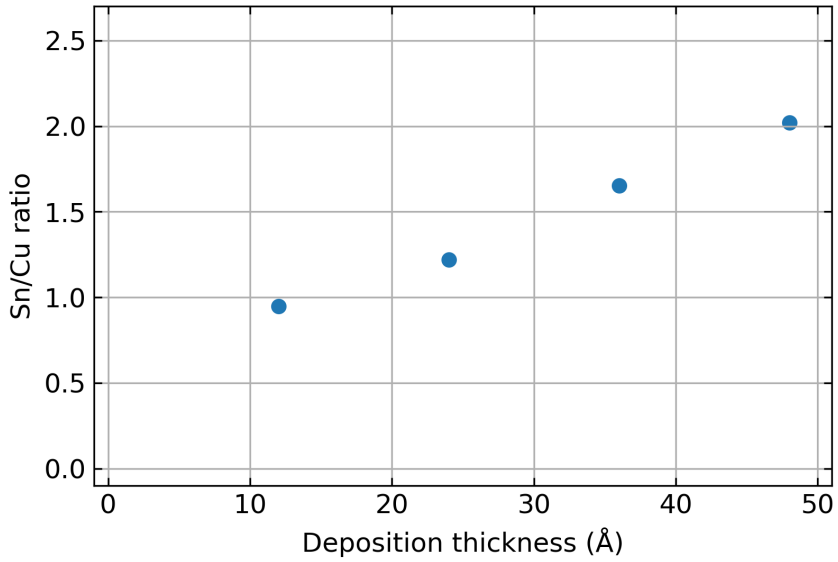

Figure 4.11: Sn/Cu ratio versus Sn deposition thickness.

4.3 Hydrogen exposure of Sn-Cu sample

The Sn-Cu sample was exposed to hydrogen gas at a pressure of $1 \cdot 10^{-4}$ mbar for different durations. In Figure 4.12 the XPS spectra of before the exposure and after the consecutive exposures can be found.

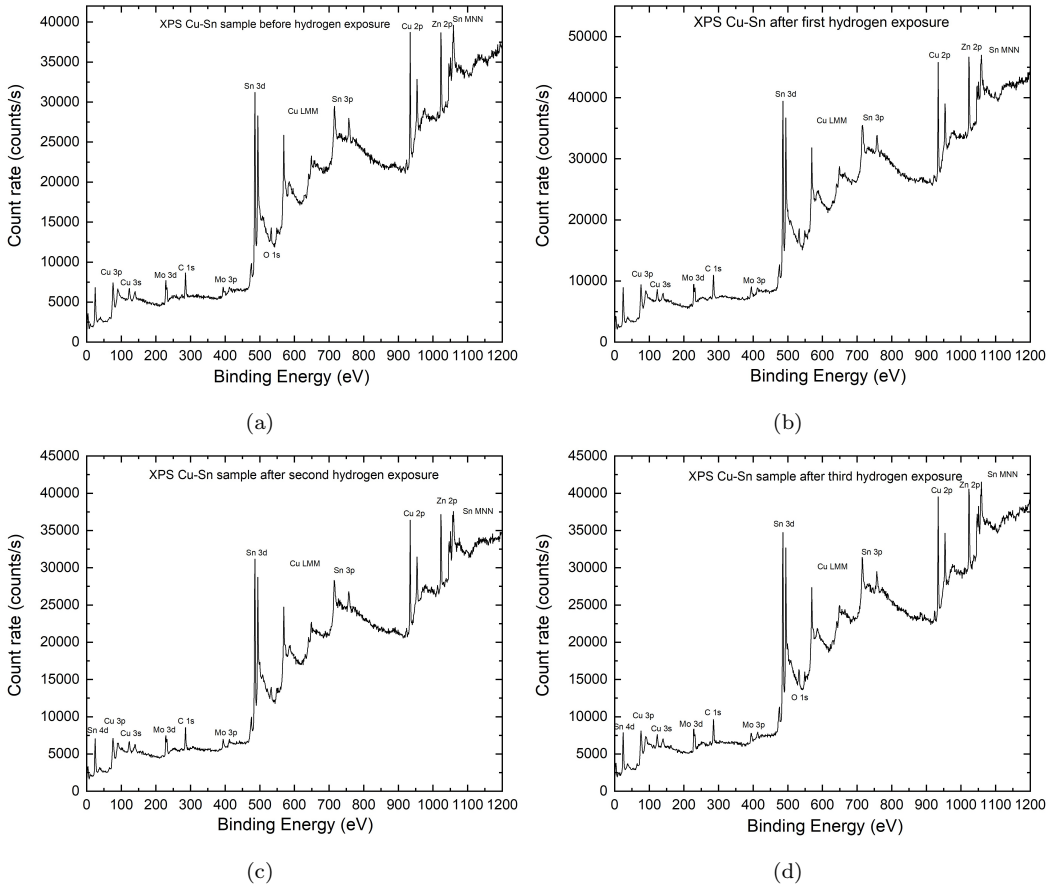

Figure 4.12: XPS spectra of the Sn-Cu sample (a) before and after three consecutive hydrogen exposures at $1 \cdot 10^{-4}$ mbar of (b) 45 min (c) 60 min and (d) 80 min.

The XPS spectra in Figure 4.12 can again be fitted with the XPS spectra from which the area can be determined. In Appendix A.4 these fits can be found. The percentages can again be determined with these fits which are given in Figure 4.13.

A plot with the ratio of Sn/Cu can be made from before and after the hydrogen exposures. In Figure 4.14 this plot can be seen.

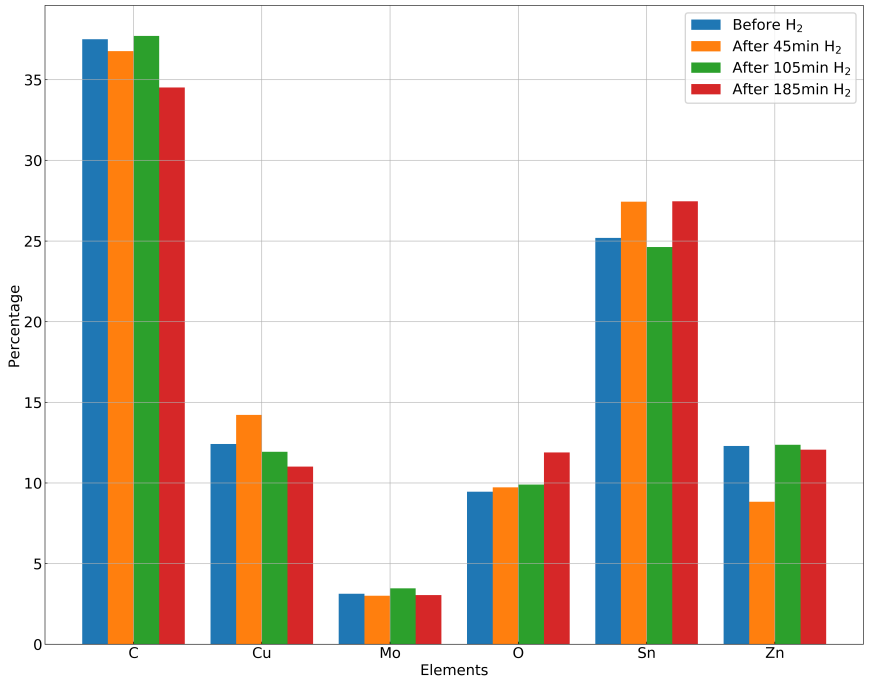

Figure 4.13: Histogram with percentages of elements detected, before and after three consecutive hydrogen exposures at $1 \cdot 10^{-4}$ mbar of 45 min, 60 min and, 80 min.

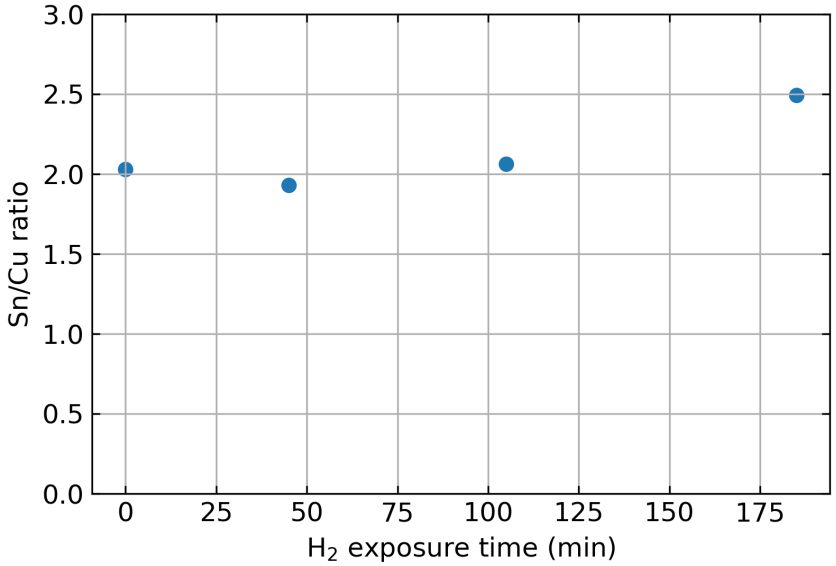

Figure 4.14: Sn/Cu ratio versus hydrogen exposure time before and after hydrogen exposures.

After the last XPS measurements were conducted an AFM examination was done again. The resulting topography images and their depth profiles can be found in Figure 4.15. It can be seen that the height variations have not changed significantly during the experiment.

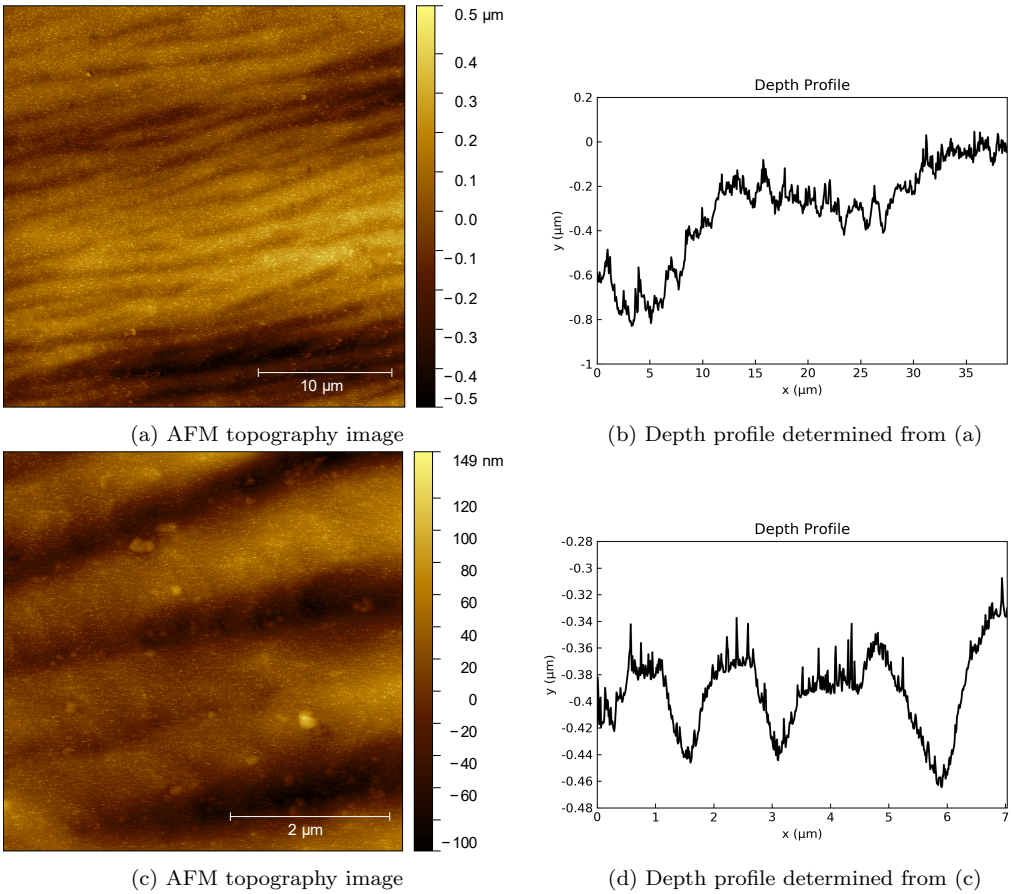

(a) AFM topography image

(b) Depth profile determined from (a)

(c) AFM topography image

(d) Depth profile determined from (c)

Figure 4.15: AFM topography images and their depth profiles at different locations of the Cu sample taken with AFM.

5. Discussion

The goal of this experiment is to set a benchmark for further research on the influence of hydrogen on Sn-covered Ru. To set a benchmark a Cu sample was covered with Sn and exposed to hydrogen.

The ratio of Sn/Cu was determined for each deposition thickness which is plotted in Figure 4.11. A clear linear relation can be seen here. However, if a line would be drawn through the data points it would not go to zero. It is expected that the ratio is zero when no Sn is deposited, and that infinity is reached when no more Cu can be detected. The linear relation shown in Figure 4.11 thus does not hold for larger ranges of deposition thicknesses. The nonlinear behavior for small deposition thicknesses can be attributed to the initial Sn deposition process. Since the surface of the Cu sample has relatively large variations in height, it is not expected that the deposited Sn will cover the sample evenly. This will result in a nonlinear relation between the Sn/Cu ratio and the deposition thickness [12].

From the plot in Figure 4.14 it can be concluded that molecular hydrogen gas exposure does not effectively remove Sn, as there is no clear decreasing relationship. In this plot, it can be seen that the data points do not form a completely straight line. This can be attributed to the low resolution of the XPS spectra. Because of this low resolution, the exact location of the top of the peaks might not be measured accurately. The area determined by a fit of such a spectrum will thus have an unknown error. In this case, the error seems to be relatively significant as a straight horizontal line is expected, assuming no interaction between molecular hydrogen and Sn.

The quality of the sample is an important aspect that should be considered. As determined with AFM measurements the height variations on the surface sample were locally a few hundreds of nanometers, with larger variations at the grain boundaries. The collector optics used in EUV lithography has a surface that is monatomic. The sample used in this experiment is not and is also made of another material and is thus not expected to represent the collector optics' surface accurately. However, the fact that no Sn was removed with hydrogen is expected to be the same for our sample and a sample of better quality. Since hydrogen is a very small molecule it should be able to reach all Sn atoms regardless of the surface roughness of the substrate.

Despite various cleaning efforts, there was still a significant amount of C present in or on the Cu sample before the Sn depositions, as can be seen in Figure 4.7. There also seems to be an increased contribution of C in the XPS spectra after the second deposition of Sn, which decreases after the third and fourth Sn depositions. This can be seen in Figure 4.10. Assuming that the Sn filament does not contain any C, this is an interesting result, as it is expected that the Sn will cover the Cu sample containing the C. Which would result in only a reduction of C.

It was also an assumption that the Sn filament in the Knudsen cell was relatively pure Sn. This assumption was found to be wrong as significant amounts of Zn were found when taking XPS spectra. The amount of Zn found in the Sn pellet is quite small, but the evaporation temperature of Zn is lower than the evaporation temperature of Sn [13]. The contribution of the Zn that is deposited onto the sample is therefore much larger. This is most likely also the reason why the contribution of Zn decreases with more Sn depositions. It is expected that after one of the first depositions most of the Zn was already evaporated. It is unclear whether the presence of Zn has any influence on the hydrogen experiment.

Before the hydrogen exposure experiment was performed, the contribution of C in the XPS spectra had increased even more. There were three days between the Sn deposition and hydrogen exposure measurements. The sample was not removed from the vacuum system during those three days, but a significant amount of C did end up on the sample. This is most likely because CO molecules might have entered the vacuum system.

Further research is required to determine the influence of hydrogen gas on Sn with the presence of Ru. It is hypothesized that the hydrogen will be able to remove Sn from a Ru surface effectively if there is some Ru exposed to the hydrogen. From this experiment, it can be concluded that there is no effective interaction between hydrogen gas and Sn alone.

6. Conclusion

Sn was deposited onto a Cu sample, which was then exposed to molecular hydrogen for a total duration of 185 minutes at a pressure of 10^{-4} mbar. It was found that the hydrogen had no significant effect on the percentage of elements present in the sample and thus it was concluded that molecular hydrogen cannot effectively remove Sn from the sample's surface.

Interestingly, Zn was also deposited onto the Cu sample as the Sn filament was contaminated with traces of Zn. It is unclear whether this has a large influence on the experiment. Additionally, there was a significant amount of C present on the Cu sample when performing the hydrogen exposures. This C appeared after the sample had been kept in the vacuum system for 3 days. This could be a result of CO molecules entering the vacuum system.

Despite annealing the Cu sample multiple times there did not seem to be much improvement on the surface roughness of the sample. Additionally, the material of the sample is different than that of collector optics and therefore the sample does not represent the collector optics plate used in EUV lithography accurately. However, it is expected that a similar result would have been found if the sample was of top quality; as hydrogen is a small molecule surface roughness should not influence a potential Sn-H_2 interaction significantly.

To determine the influence of hydrogen gas on a Sn-covered Ru surface, further research is required. It is expected that the presence of Ru will catalyze the formation of SnH_4, as Ru is known to chemically absorb hydrogen.

Bibliography

[1] Gerry O'Sullivan, Deirdre Kilbane, and Rebekah D'Arcy. "Recent progress in source development for extreme UV lithography". In: *Journal of Modern Optics* 59 (June 2012), pp. 855–872. DOI: 10.1080/09500340.2012.678399.

[2] Oscar Versolato et al. "Microdroplet-tin plasma sources of EUV radiation driven by solid-state-lasers (Topical Review)". In: *Journal of Optics* 24 (Mar. 2022), pp. 054014–054014. DOI: 10.1088/2040-8986/ac5a7e.

[3] Daisuke Nakamura et al. "Mitigation of fast ions generated from laser-produced Sn plasma for extreme ultraviolet light source by H2 gas". In: *Journal of Applied Physics* 102 (Dec. 2007), pp. 123310–123310. DOI: 10.1063/1.2818026.

[4] Tao Wu et al. "Debris mitigation power of various buffer gases for CO_2 laser produced tin plasmas". In: *Journal of Physics* 45 (Nov. 2012), pp. 475203–475203. DOI: 10.1088/0022-3727/45/47/475203.

[5] Daniel T Elg et al. "*In situ* collector cleaning and extreme ultraviolet reflectivity restoration by hydrogen plasma for extreme ultraviolet sources". In: *Journal of Vacuum Science Technology A: Vacuum, Surfaces, and Films* 34 (Feb. 2016), pp. 021305–021305. DOI: 10.1116/1.4942456.

[6] Klaus Christmann. "Interaction of hydrogen with solid surfaces". In: *Surface Science Reports* 9 (July 1988), pp. 1–163. DOI: 10.1016/0167-5729(88)90009-x.

[7] John F Moulder and Jill Chastain. *Handbook of x-ray photoelectron spectroscopy : a reference book of standard spectra for identification and interpretation of XPS data*. Perkin-Elmer Corporation, 1992.

[8] Leonard C Feldman and James W Mayer. *Fundamentals of Surface and Thin Film Analysis*. Elsevier Science Publishing B.V., 1986.

[9] Carlos D Wagner et al. "Empirical atomic sensitivity factors for quantitative analysis by electron spectroscopy for chemical analysis". In: *Surface and Interface Analysis* 3 (Oct. 1981), pp. 211–225. DOI: 10.1002/sia.740030506.

[10] E. Meyer. "Atomic force microscopy". In: *Progress in Surface Science* 41 (Sept. 1992), pp. 3–49. DOI: 10.1016/0079-6816(92)90009-7.

[11] Varun Jain, Mark C. Biesinger, and Matthew R. Linford. "The Gaussian-Lorentzian Sum, Product, and Convolution (Voigt) functions in the context of peak fitting X-ray photoelectron spectroscopy (XPS) narrow scans". In: *Applied Surface Science* 447 (July 2018), pp. 548–553. DOI: 10.1016/j.apsusc.2018.03.190. URL: https://www.surfacesciencewestern.com/wp-content/uploads/ass18_biesinger.pdf.

[12] Sven Tougaard. "Practical guide to the use of backgrounds in quantitative XPS". In: *Journal of Vacuum Science Technology A* 39 (Jan. 2021), p. 011201. DOI: 10.1116/6.0000661.

[13] *Vacuum Deposition Techniques and Tables*. www.tedpella.com. URL: https://www.tedpella.com/company_html/vacuum-deposition-techniques-and-tables.aspx.

A. Appendix

A.1 Atomic sensitivity factors

In the following table, the relevant atomic sensitivity factors are given, determined according to Section 2.1.3.

Table A.1

Orbital	ASF for X-ray source at 30°.
C 1s	0.30
Cu 2p	5.97
Mo 3d	3.89
O 1s	0.71
Sn $3d_{5/2}$	5.51
Zn $2p_{3/2}$	4.19

A.2 AFM depth profiles

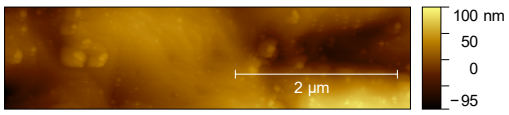

(a) AFM topography image

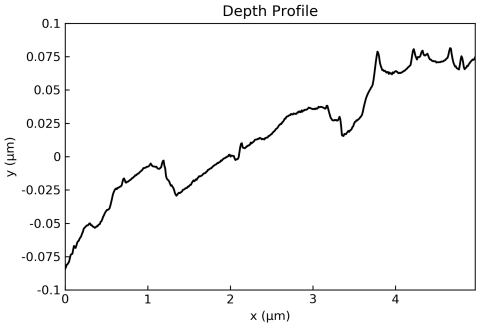

(b) Depth profile determined from (a)

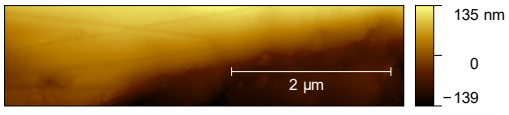

(c) AFM topography image

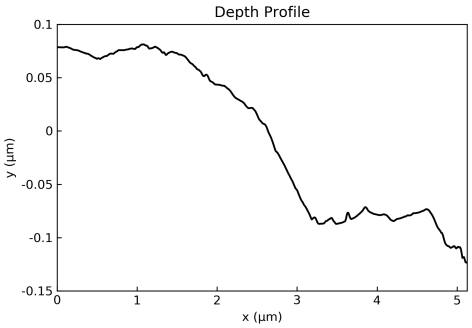

(d) Depth profile determined from (c)

Figure A.1: AFM topography images and their depth profiles at different locations of the Cu sample taken with AFM.

A.3 XPS spectrum Sn pellet

In Figure A.2 the XPS spectrum and its Zn detail can be found, it can be seen that the percentage of Zn in this spectrum is relatively small compared to Sn.

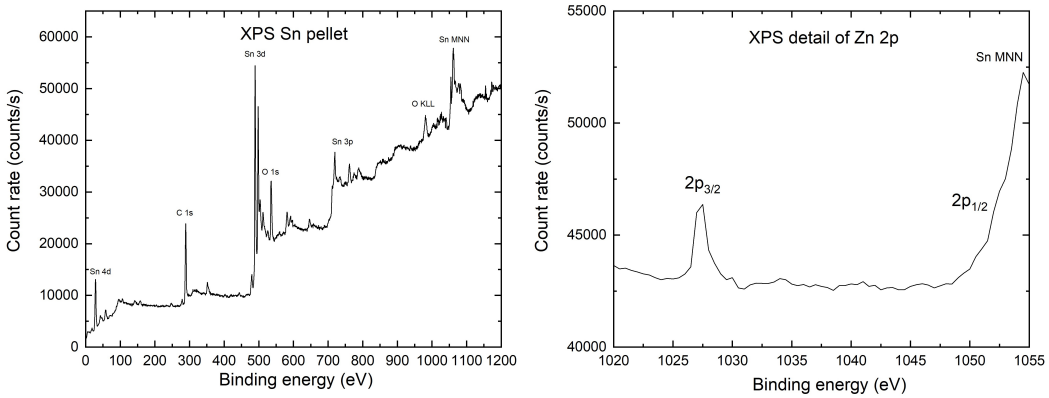

(a) XPS spectrum of Sn pellet

(b) XPS detail of the Zn peaks

Figure A.2: XPS measurement of an Sn pellet.

A.4 XPSPEAK41 fits

In the following figures the XPSPEAK41 fits of relevant peaks from the XPS spectra can be found.

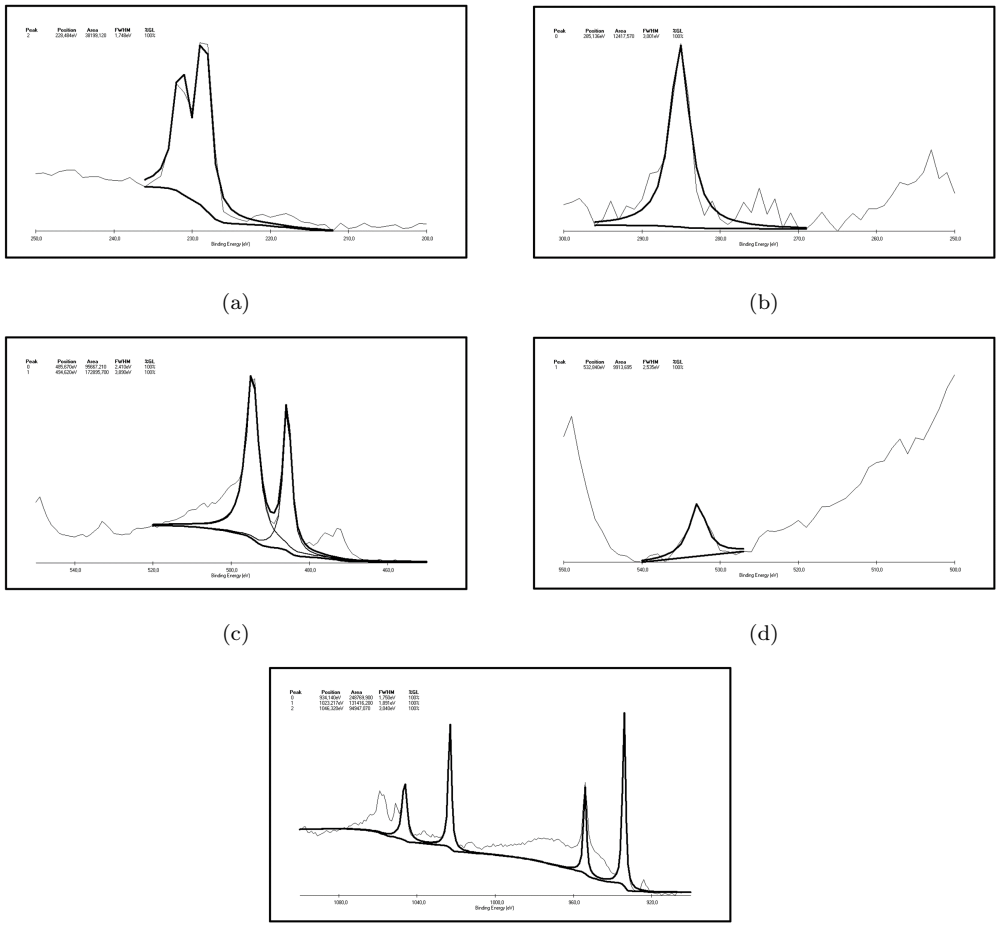

Figure A.3: XPSPEAK41 fits after the first Sn deposition of the following peaks (a) Mo, 200-250 eV (b) C, 250-300 eV (c) Sn, 450-550 V (d) O, 500-550 eV(e) Cu and Zn, 900-1100 eV.

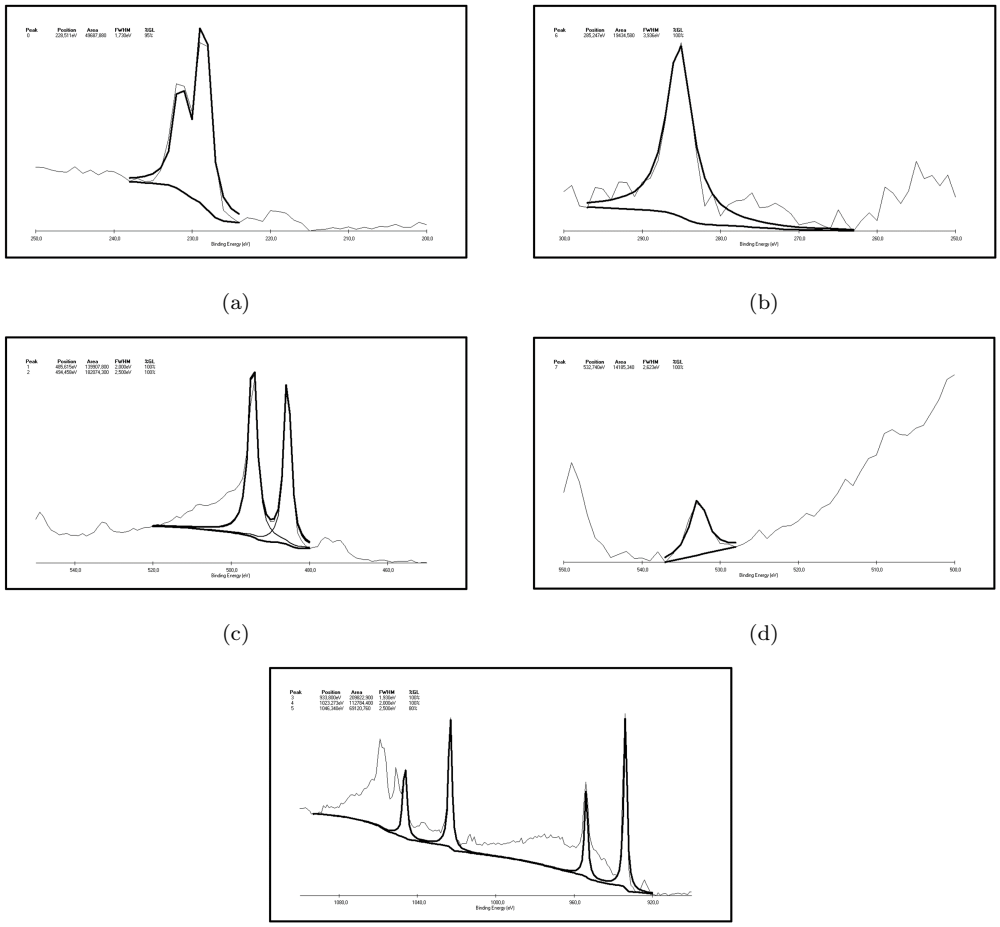

(a) (b) (c) (d) (e)

Figure A.4: XPSPEAK41 fits after the second Sn deposition of the following peaks (a) Mo, 200-250 eV (b) C, 250-300 eV (c) Sn, 450-550 V (d) O, 500-550 eV(e) Cu and Zn, 900-1100 eV.

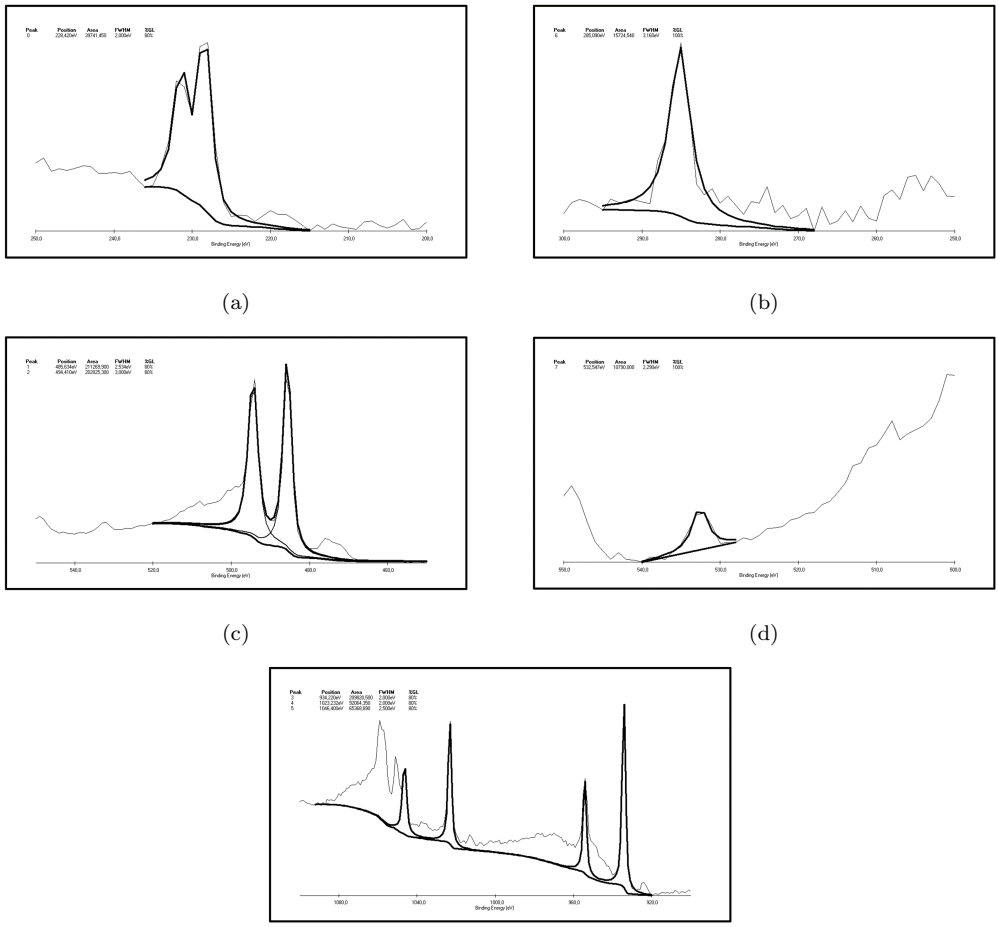

(a) (b) (c) (d) (e)

Figure A.5: XPSPEAK41 fits after the third Sn deposition of the following peaks (a) Mo, 200-250 eV (b) C, 250-300 eV (c) Sn, 450-550 V (d) O, 500-550 eV(e) Cu and Zn, 900-1100 eV.

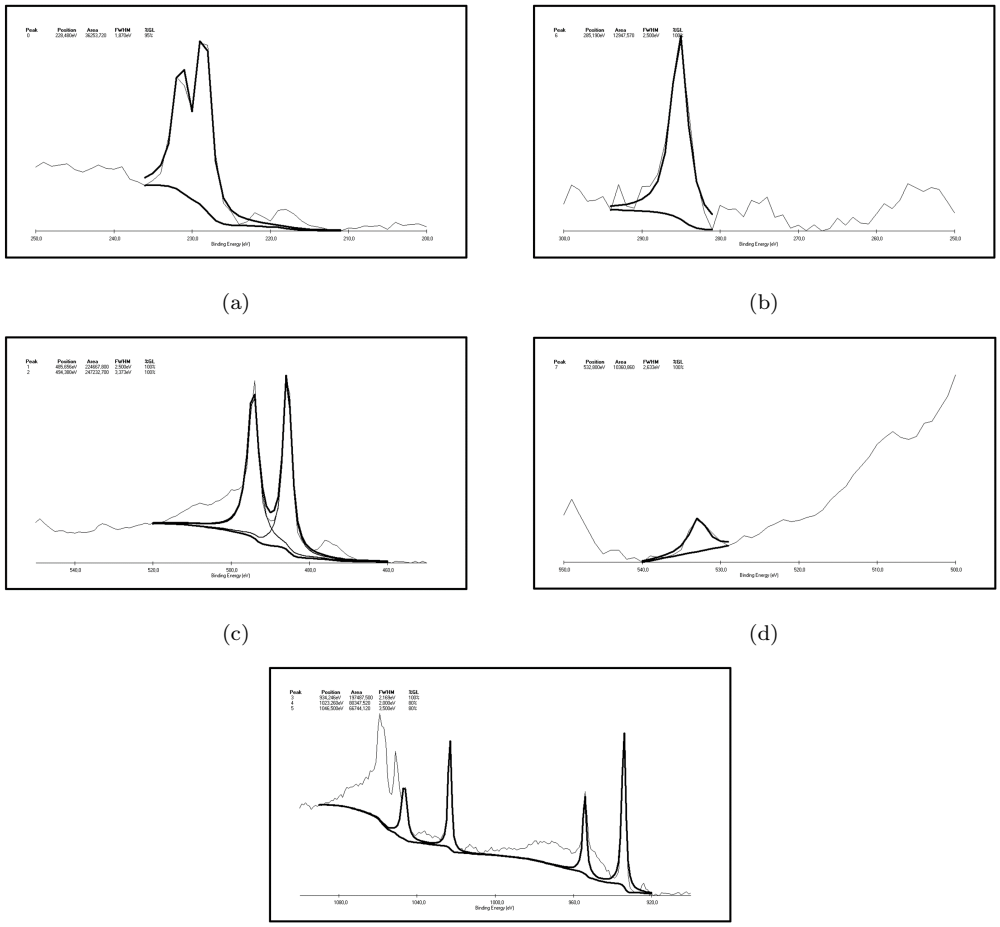

(a) (b) (c) (d) (e)

Figure A.6: XPSPEAK41 fits after the fourth Sn deposition of the following peaks (a) Mo, 200-250 eV (b) C, 250-300 eV (c) Sn, 450-550 V (d) O, 500-550 eV(e) Cu and Zn, 900-1100 eV.

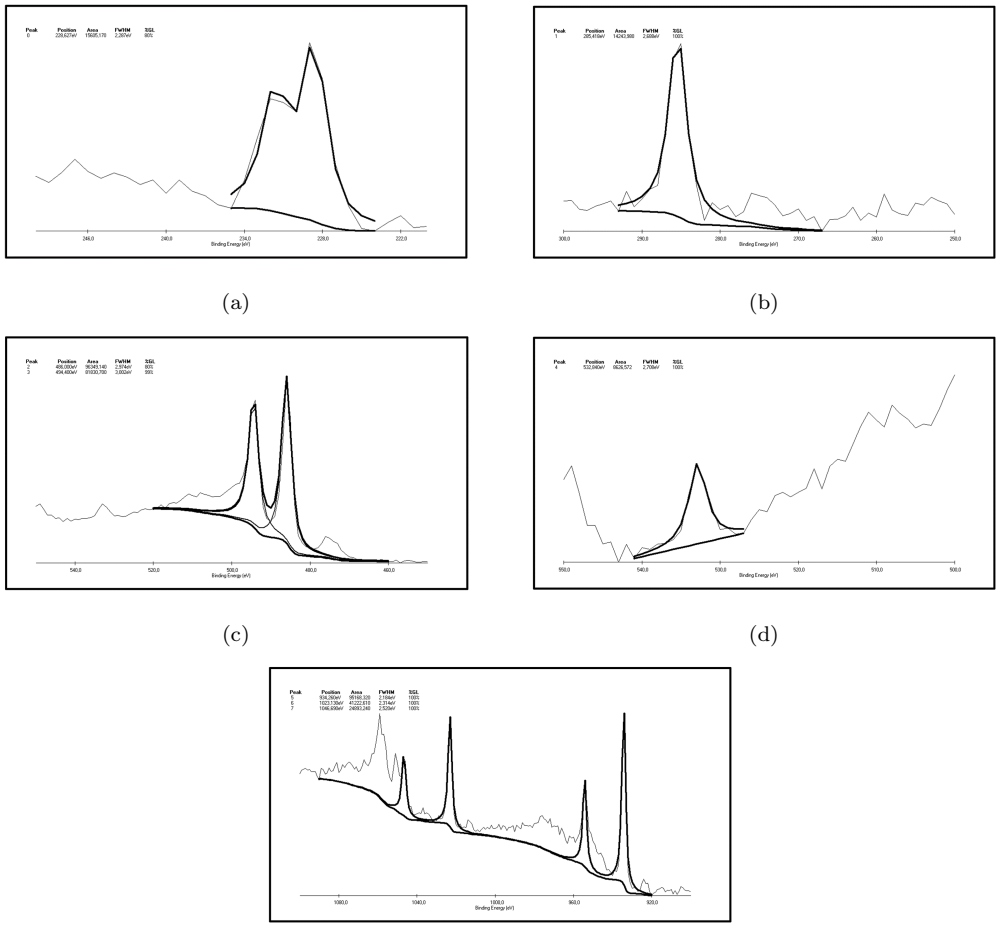

(a) (b) (c) (d) (e)

Figure A.7: XPSPEAK41 fits before the first hydrogen exposure of the following peaks (a) Mo, 220-250 eV (b) C, 250-300 eV (c) Sn, 450-550 V (d) O, 500-550 eV(e) Cu and Zn, 900-1100 eV.

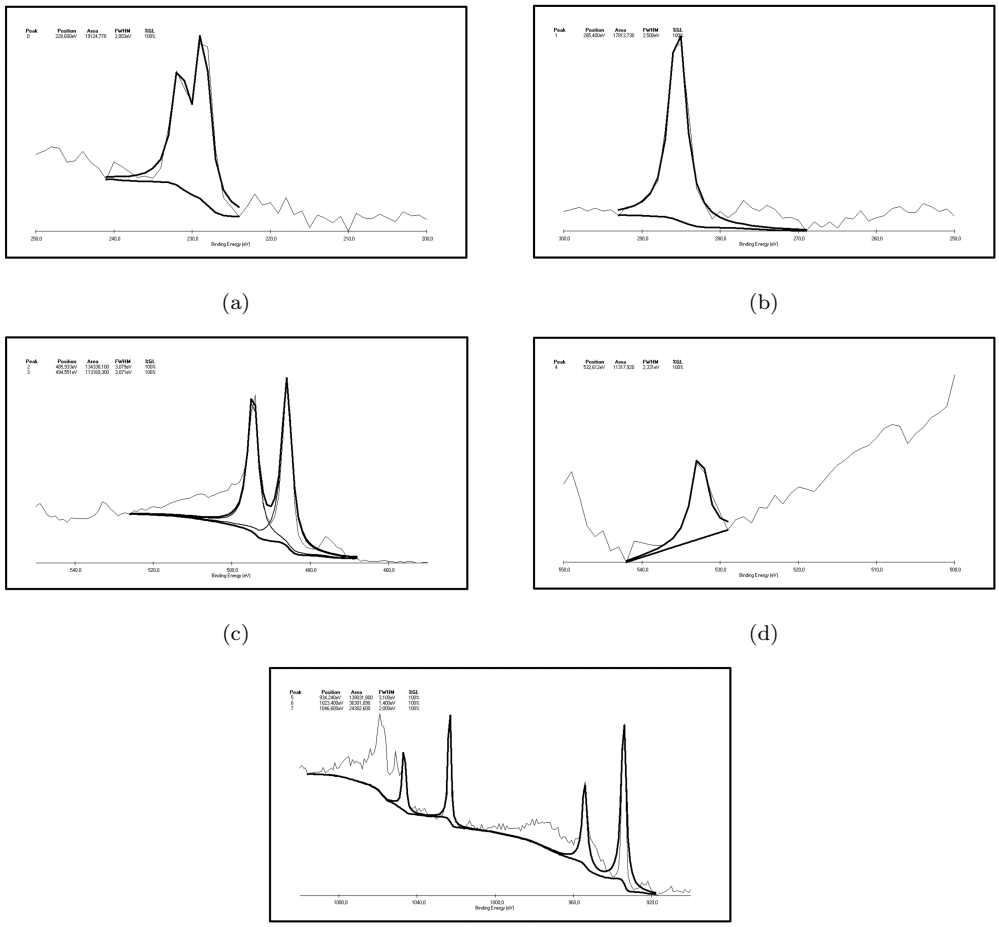

(a) (b) (c) (d) (e)

Figure A.8: XPSPEAK41 fits after the first hydrogen exposure of the following peaks (a) Mo, 200-250 eV (b) C, 250-300 eV (c) Sn, 450-550 V (d) O, 500-550 eV(e) Cu and Zn, 900-1100 eV.

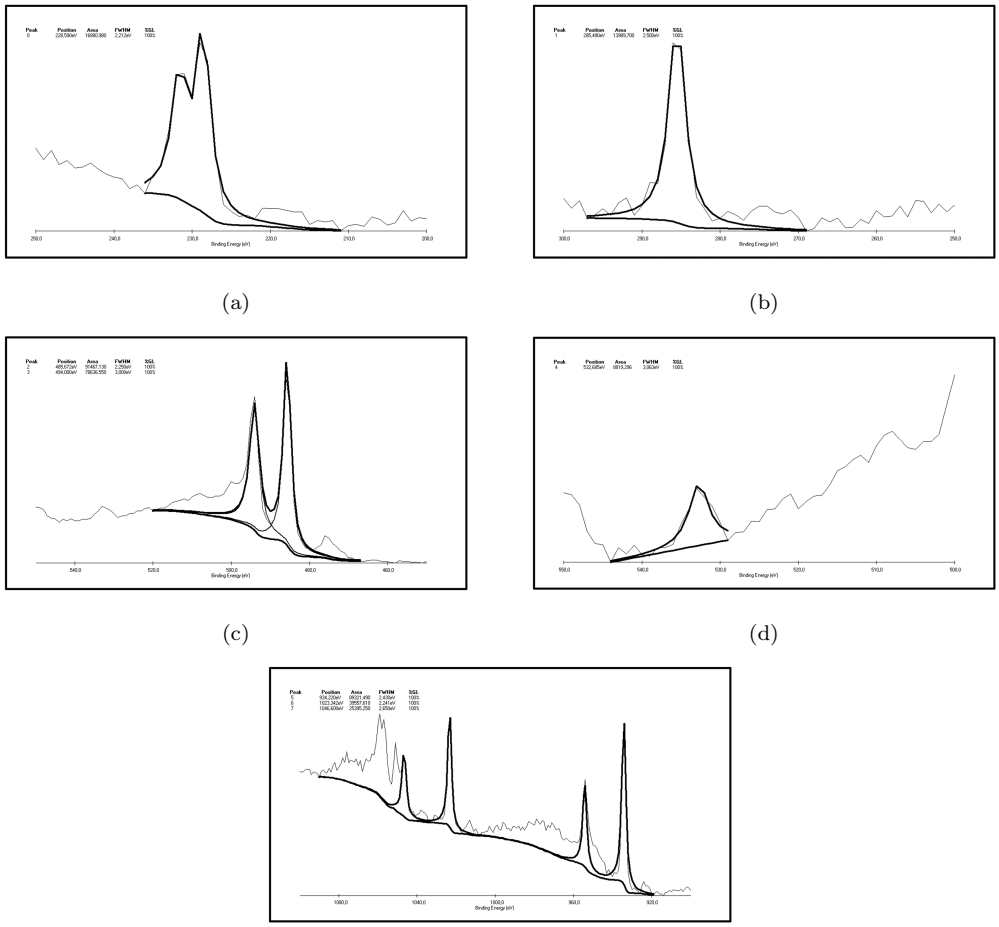

(a) (b) (c) (d) (e)

Figure A.9: XPSPEAK41 fits after the second hydrogen exposure of the following peaks (a) Mo, 200-250 eV (b) C, 250-300 eV (c) Sn, 450-550 V (d) O, 500-550 eV(e) Cu and Zn, 900-1100 eV.

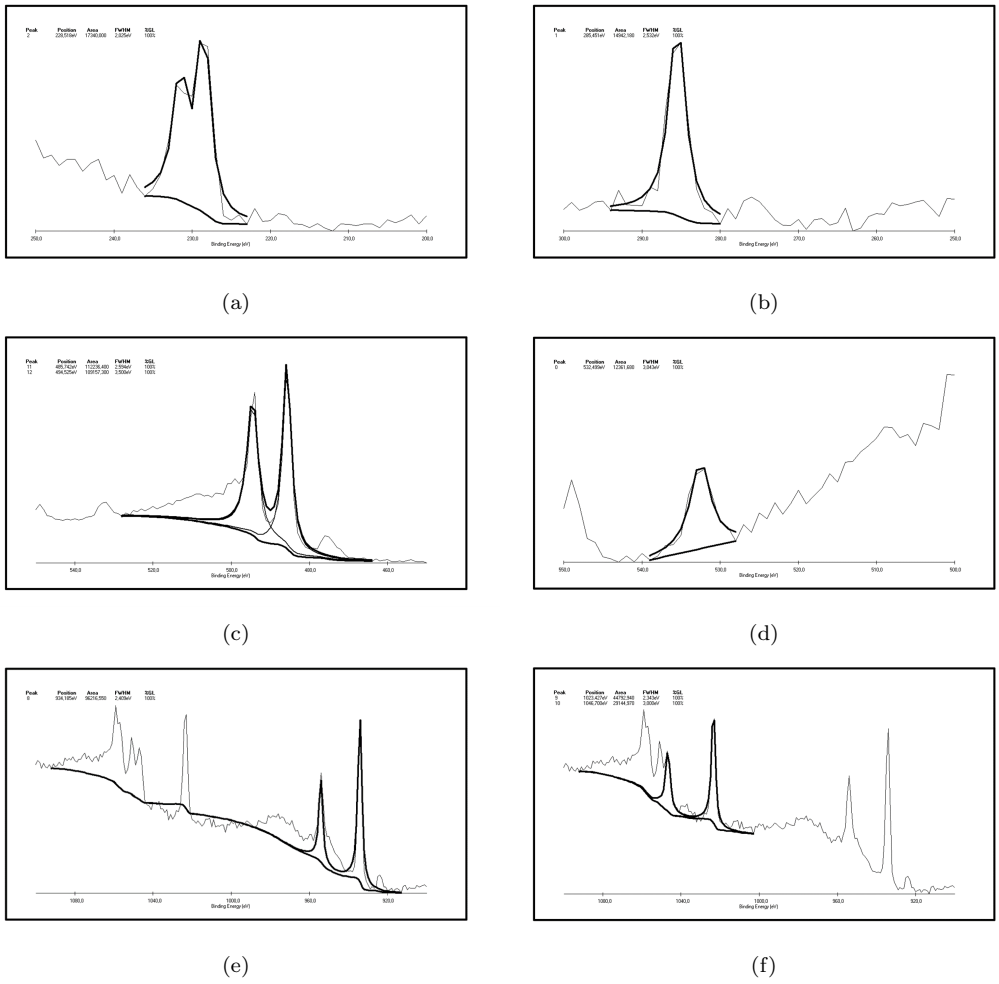

(a) (b)

(c) (d)

(e) (f)

Figure A.10: XPSPEAK41 fits after the third hydrogen exposure of the following peaks (a) Mo, 200-250 eV (b) C, 250-300 eV (c) Sn, 450-550 V (d) O, 500-550 eV(e) Cu and Zn, 900-1100 eV.